Combined Use of Sentinel-1 and Sentinel-2 for Burn Severity Mapping in a Mediterranean Region

Giandomenico De Luca[1], João M. N. Silva[2], Duarte Oom[2,3P], and Giuseppe Modica[1(✉)]

[1] Dipartimento Di Agraria, Università Degli Studi Mediterranea Di Reggio Calabria, Località Feo di Vito, 89122 Reggio Calabria, Italy
{giandomenico.deluca,giuseppe.modica}@unirc.it
[2] Forest Research Centre, School of Agriculture, University of Lisbon, Tapada da Ajuda, 1349-017 Lisboa, Portugal
joaosilva@isa.ulisboa.pt
[3] European Commission, Joint Research Centre, Ispra Site, Ispra, Italy
Duarte.Oom@ec.europa.eu

Abstract. The present study is focused on investigating the capabilities of the combined use of synthetic aperture radar (SAR) Sentinel-1 (S1) and optical Sentinel-2 (S2) for burn severity mapping. For this purpose, a fire that occurred in August 2018 in southern Portugal was analyzed. The composite burn index (CBI) was used to visually classify geo-referenced photographs in the field and create the training data for image classification. A supervised classification was carried out using the machine learning random forests (RF) algorithm, on which the optimization of the parameters setting was carried out through an exhaustive grid search approach. In order to assess the advantages of combining optical and SAR data, and the importance of each band, the approach was tested separately on three data combinations (S1, S2 and S1 + S2) and feature importance was computed to evaluate the contribution of each input layer. The multi-class F-score, used to assess the accuracy of the map, reached a value of 0.844 when both the datasets were combined (S1 + S2), compared with the values 0.514 and 0.805 achieved by only SAR (S1) and only optical (S2), respectively.

Keywords: Composite burn index (CBI) · Random forest (RF) · Exhaustive grid search (GridSearchCV) · Scikit-learn · SNAP-Python (snappy) interface

1 Introduction

Wildfires are one of the most important ecological factors in Mediterranean ecosystems, with different degrees of impact depending on the severity and distribution of burns [1–6]. These effects determine, at different spatial and temporal scales, microclimatic and ecological changes that rearrange the habitats assets, positively (i.e., regeneration, regrowth, vegetation composition enrichment) or negatively (i.e., degradation, desertification, higher exosystemic vulnerability) [1, 4, 7–12]. Burn severity is defined as the

© Springer Nature Switzerland AG 2021
O. Gervasi et al. (Eds.): ICCSA 2021, LNCS 12955, pp. 139–154, 2021.
https://doi.org/10.1007/978-3-030-87007-2_11

degree of environmental change caused by fire, analytically measured as the degree of chemical-physical changes, decomposition and loss of above/belowground organic matter [13, 14]. It influences and determines, at various degrees, the transformation of the organic and mineral components of the soil, the conversion of biomass into inorganic carbon, structural transformation of habitats and, at the most extreme degree, the destruction of the biological communities of an ecosystem [14]. The spatial distribution of the burn severity is a crucial and essential step for assessing and monitoring the impacts of fire on ecosystems and addressing optimal and timely post-fire management operations [2, 7, 10, 15–17]. Key & Benson [14] proposed the composite burn index (CBI) for determining the burn severity, becoming a standard metric in literature. This index is based on the qualitative/quantitative measurement of ecosystem alterations and carried out through visual interpretation in sample field plots, comparing the aboveground biomass and necromass after the fire with their pre-fire conditions. In the CBI protocol, several ecological attributes are measured to estimate the effect of fire in the post-fire environment in five vertical structural layers (strata): litter and duff consumption, canopy cover reduction, branch and wood consumption and plant mortality [13, 14, 18].

Remote sensing techniques and satellite data are effective when retrieving the spatial distribution over large areas of the burn severity information carried out in the field plots, with a high level of correlation [2, 13, 16, 19–21]. Their use was encouraged by the availability of open-source data, acquired from satellite sensors with increasing spatial and temporal resolutions [22, 23], and software that provides advanced process and analysis tools. In this context, the Sentinel constellation (Copernicus mission) launched by the European Space Agency (ESA) provides free high temporal and spatial resolution data acquired by several sensors. The Sentinel-1 (S1) and Sentinel-2 (S2) missions consist, respectively, of a C-band synthetic aperture radar (SAR) and an optical multispectral sensor, both composed of two polar-orbiting satellites (S1A/B and S2A/B) [24].

The high sensitivity in the visible, near-infrared (NIR) and short-wave infrared (SWIR) spectral bands to the effects of fire on ecosystems [25, 26] allowed the rapid development and diffusion of optical-based approaches for this purpose, achieving efficient results [10, 22, 27–30]. In the past decades, numerous authors proposed different methods aimed at estimating and mapping burn severity using remotely sensed data [2–4, 17, 27, 31–33] and effective vegetation indices using optical sensors [2, 34–38]. SAR data have also been explored in recent years for burn severity mapping [39–42]. Tanase et al. [43] and Tanase et al. [44] explored the suitability of different frequency SAR sensors for burn severity purposes in Mediterranean vegetation. Tanase et al. [21] proposed a SAR index to estimate fire severity in temperate forests, based on the ratio between post and pre-fire SAR images. The sensitivity of SAR signal is given by the variation in vegetation and soil structure and moisture content, which affect the dielectric properties of the surface and influence the level of microwave backscatter, in synergy with various environmental factors and/or intrinsic sensors characteristics (e.g., wavelength and polarization) [44, 45]. Therefore, this type of active sensor may be a complementary source for monitoring the fire impacts on ecosystems, considering that it is not sensitive to cloud cover conditions [46–49]. However, few studies focused on integrating the two types of sensors for the estimation of burnt area [48, 50] and, even less, for burn severity [51].

This study aims to contribute to the state of the art by evaluating the capability of the integrated use of S1 and S2 to estimate burn severity using the random forest (RF) machine learning algorithm and the field-based CBI measurements as training data. A series of processing steps anticipated the severity estimation: a) download and preprocessing of optical and SAR time series and subsequent creation of input image layers; b) creation of three dataset combinations: S1, S2 and S1 + S2, in order to evaluate the contribution of each sensor to the final accuracy; c) search and setting of optimal values of RF parameters using an exhaustive grid search approach. The single and multi-class F-score was calculated to assess the accuracy of the maps. The feature importance was extracted to evaluate each input variable's contribution to the final map accuracy. All the processes were carried out using open-source software and libraries executed in python-script language [52].

2 Study Area

The study area is located in the south of Portugal (Algarve, 37° 18′N; 08° 30′W), in the Serra de Monchique mountain range. The site is characterized by typical Mediterranean vegetation. The forest areas were composed of coniferous (*Pinus pinea* L., *Pinus pinaster* Aiton.), broad-leaves trees (*Quercus suber* L., *Quercus ilex* L., other secondary Mediterranean native species), and Eucalyptus plantations (*Eucalyptus globulus*, Labill. 1800). A large part of the territory is covered by sclerophyllous shrublands or pastures, interspersed with agricultural and urban landscapes [53]. The fire event occurred in August from the 3rd to the 10th of 2018, covering 268.9 km^2 (Fig. 1).

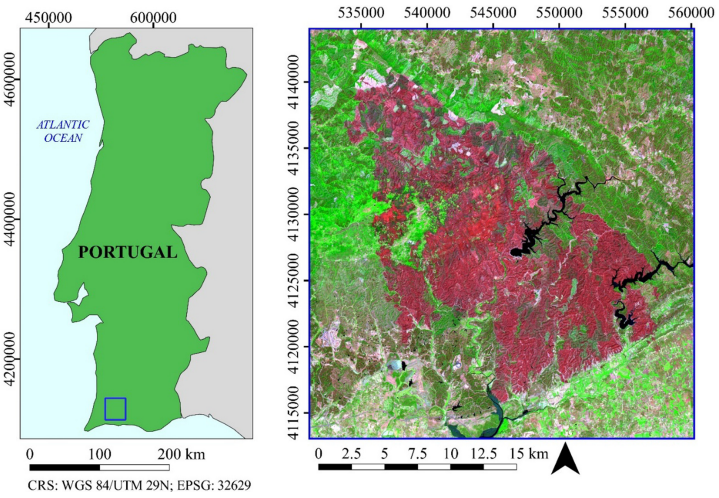

Fig. 1. Location of the study burned area in Portugal (on the left). On the right, overview of the study area (Sentinel-2 image on August 13th, 2018 false-colour composite SWIR-NIR-RED), where the red area represents the burned area.

3 Materials and Methods

3.1 Satellite Datasets

The SAR dataset was composed of a temporal series of Sentinel-1A/B ground range detected (GRD), acquired in interferometric wide (IW) mode, dual-polarized (vertical-vertical VV, and vertical-horizontal VH polarizations). Five images for the pre-fire period (covering around the month before the event starting date) and five images for the post-fire period (covering the period from the end of the event until the end of the same month), including both the ascending and descending orbits (Table 1).

Table 1. The Sentinel-1 dataset used in this study. The red lines separate the images acquired before and after the fire.

Mission	Orbit	Product	Sensing Date
S1A	Ascending	IW Level-1 GRDH	2018/07/07
S1A	Descending		2018/07/08
S1A	Ascending		2018/07/19
S1A	Descending		2018/07/20
S1A	Ascending		2018/07/31
S1A	Ascending		2018/08/12
S1B	Ascending		2018/08/18
S1A	Ascending		2018/08/24
S1A	Descending		2018/08/25
S1B	Ascending		2018/08/30

The optical dataset was composed of a temporal series of Sentinel-2A/B Level 2A (Bottom of Atmosphere reflectance), composed of three images before and three images after the fire (accounting for a similar time frame to that considered for the S1 dataset). Both S1 and S2 images were downloaded through the [54] (Table 2).

Table 2. The Sentinel-2 dataset used in this study. The red lines separate the images acquired before and after the fire.

Mission	Product	Sensing Date
S2A	Level-2A MS	2018/07/09
S2A		2018/07/19
S2A		2018/07/29
S2B		2018/08/13
S2A		2018/08/18
S2B		2018/08/23

3.2 Field Data and ROIs Selection

The field sampling involved capturing post-fire conditions through geo-referenced photographs in different points sampled on the burned surface. Field data were collected

in November of the same year of the fire (2018), before the growing season, to avoid confusion between regenerated and unburned vegetation. Fire severity quantification was based on the visual interpretation of the photographs, supported by the Esri ArcGIS World Imagery map [55], providing post-fire medium/high-resolution images and by the field notes taken during the on-field surveys. The protocol used in this study to quantify fire severity was the Composite Burn Index (CBI), consisting of visually estimation of post-fire change in several ecological variables for each of the five vegetation stratum (inert understory substrate and fuel; herbs, low shrubs and $<1\ m$ high trees; tall shrubs and $<5\ m$ high trees; subcanopy intermediate trees; dominant and codominant cover trees). The level of changed inducted by the fire was ranked between 0 (unburned) and 3 (highest level of severity). The average of all the index values for each variable and stratum represented the severity CBI value of the entire single plot observed. Based on the CBI values obtained, six fire severity categories were created: 1) Unburned soil/rock; 2) Unburned vegetation; 3) Low severity; 4) Moderate severity; 5) Moderate-High severity; 6) High severity. During the field surveying, 200 sampling photographs were taken, from which 185 sampling plots were observed. Each of these points was the centre of a 20 m $\times$ 20 m square sampling area (region of interest, ROI), homogeneous in terms of burn severity, matching 2 $\times$ 2 pixel areas on Sentinel images (considering resampling of the pixels at 10 m; see Subsect. 3.3). Each ROI was finally labelled with one of the six severity categories.

3.3 Satellite Data Pre-processing and Layers Creation

The data pre-processing was carried out using the Sentinel-1 and Sentinel-2 Toolboxes implemented in the SNAP v.8.0.1 open-source software [56] provided by ESA and executed through Snappy [57], the SNAP-Python interface.

S1. The S1 pre-processing workflow started from the auto-downloaded orbit file application and the thermal noise removal. After the radiometric calibration to beta (β0) noughts backscatter standard conventions, the radiometric terrain correction (RTC) process was applied to the dataset, flattening (radiometric terrain flattening) and geometrically correcting (terrain correction) the images using the shuttle radar topography mission (SRTM) digital elevation model (DEM), presenting a spatial-sampling of 1 arc-second. The bilinear interpolation resampling method was used for both DEM and output image resampling. All the S1 images were stacked using the product geolocation as the initial offset method. A multitemporal Lee filter [58, 59], with a 5 $\times$ 5 pixel window size, was applied to reduce speckle noise effects. The backscatter time average (BTA) was computed separately for the images before and after the event and for polarization to improve speckle reduction [15, 21, 41]. From the four resulted BTA image layers, three S1-adapted dual-polarimetric SAR indices were computed to have layers expressing the two polarizations' combination [60–62]:

$$RVI_t = 4 \cdot BTA_VH_t/(BTA_VV_t + BTA_VH_t) \tag{1}$$

$$DPSVI_t = (BTA_VV_t + BTA_VH_t)/BTA_VV_t) \tag{2}$$

$$RFDI_t = (BTA_VV_t - BTA_VH_t)/(BTA_VV_t + BTA_VH_t) \tag{3}$$

Where *t* represents one of the two time periods: before or after the fire.

Moreover, the difference between pre- and post-fire of each respective image layer was computed (Δ = pre-fire – post-fire). In the end, the $BTA_VH_{post\text{-}fire}$, ΔBTA_VH, $BTA_VV_{post\text{-}fire}$, ΔBTA_VV, $RVI_{post\text{-}fire}$, ΔRVI, $DPSVI_{post\text{-}fire}$, ΔDPSVI, $RFDI_{post\text{-}fire}$, ΔRFDI formed the SAR-based input image layers in the next classification steps.

S2. The S2 pre-processing concerned the pixel resampling to 10 m × 10 m pixel size. As with the S1 dataset, the time average was computed for the images before and after the fire. All 10 m and 20 m spatial resolution, and their respective pre- and postfire difference (Δ), were used as image input layers in the classification processes: B2 (Blue), ΔB2, B3 (Green), ΔB3, B4 (Red), ΔB4, B5 (RedEdge1), ΔB5, B6 (RedEdge2), ΔB6, B7 (RedEdge3), ΔB7, B8 (NIR), ΔB8, B8A (NarrowNIR), ΔB8A, B11 (SWIR1), ΔB11, B12 (SWIR2), ΔB12.

The two S1 and S2 datasets, clipped on the same area, were stacked together using the S1 dataset as the master extent. The bilinear interpolation was performed to resample the pixels between master and slaves.

3.4 Image Classification

The random forests (RF) algorithm [63, 64] was used to perform a supervised pixel-based classification, using a part (2/3) of the pixels contained and labeled in the ROIs (described in Subsect. 3.2) as training data. Three different dataset combinations were evaluated: only optical (S2); only SAR (S1); optical and SAR (S1+S2). To assess each image layer's contribution to the classification, the feature importance (Gini importance) was computed for each of the three dataset combinations. The classification algorithm was implemented in the scikitlearn library (*RFclassifier* module) [65] and executed via a Python script.

Parameters optimization. The optimal values of the algorithm parameters were determined using an exhaustive grid search approach. The exhaustive grid search is based on testing and cross-validation of each possible combination of the set of values given for each parameter, returning the best combination for a given training input set. The *GridSearchCV* algorithm implemented in scikit-learn was used for this purpose. The combination of parameters tested is reported in Table 3.

3.5 Accuracy Assessment

The remainder of ROIs pixels (1/3) was used to validate the classification accuracy of the three burn severity maps (S2, S1 and S1+S2). The confusion matrix was carried out, from which the *producer's* accuracy (defined as the ratio between the correctly classified pixels in a given class and the number of validation pixels for that class) and the *user's* accuracy (the ratio between the correctly classified pixels in a given class and all the classified objects in that class) were calculated [66]. From these measures, we calculated the single-class F-score ($F\text{-}score_i$) (Eq. 4) [15, 67–71] and the multi-class F-score ($F\text{-}score_M$) (Eq. 5) [73], representing a form of overall accuracy. The F-score is the harmonic mean of *recall* and *precision* measures, which have the same respective

Table 3. Sets of parameters values tested and combined for exhaustive grid search-based optimization. The name and the definition of each parameter are the original ones reported in the *RFclassifier* module user guide.

Parameter name	Values set	Description
n_estimators	100, 650, 1200, 1750, 2300, 2850, 3400, 3950, 4500, 5050, 5600, 6150, 6700, 7250, 7800, 8350, 8900, 9450, 10000	The number of trees in the RF model
max_depth	10, 20, 30, 40, 50, 60, 70, 80, 90, 100, 110, 300, 500, 800, 1000	The maximum depth of the tree
min_samples_split	2, 5, 10	The minimum number of samples required to split an internal node
min_samples_leaf	1, 2, 4	The minimum number of samples required to be at a leaf node
max_features	"auto", "None", "log2"	The number of features to consider when looking for the best split

meaning of *producer's* and *user's* accuracy. Therefore they were replaced in the equations (Eq. 4, 6, 7) [73].

$$F-score_i = 2 \cdot \left(producer's_i \cdot user's_i\right) / \left(producer's_i + user's_i\right) \tag{4}$$

$$F-score_M = 2 \cdot \left(producer's_M \cdot user's_M\right) / \left(producer's_M + user's_M\right) \tag{5}$$

Where i is a single class; $producer's_M$ and $user's_M$ metrics are expressed as follows (Eq. 6, 7):

$$producer's_M = \left(\sum_{i=1} producer's_i\right) / n \tag{6}$$

$$user's_M = \left(\sum_{i=1} user's_i\right) / n \tag{7}$$

Where n is the total number of classes.

4 Results

4.1 Classified Burn Severity Map

Table 4 shows the RF classification algorithm's optimal parameters values, set using an exhaustive grid search approach. This was carried out for each of the three data combination (S1, S2 and S1+S2) separately.

Figure 2 shows the three burn severity maps resulted from the classification processes tested: only S1, only S2 and S1+S2, respectively.

In Table 5, the distribution (%) of the area of each burn severity classes is reported.

Table 4. Random forests (RF) parameters values used for each of the three data combinations (S1, S2 and S1 + S2) and set using an exhaustive grid search approach.

Parameter name	Values set		
	S1	S2	S1+S2
n_estimators	650	1200	1200
max_depth	1000	90	110
min_samples_split	2	2	2
min_samples_leaf	1	1	1
max_features	"log2"	"auto"	"auto"

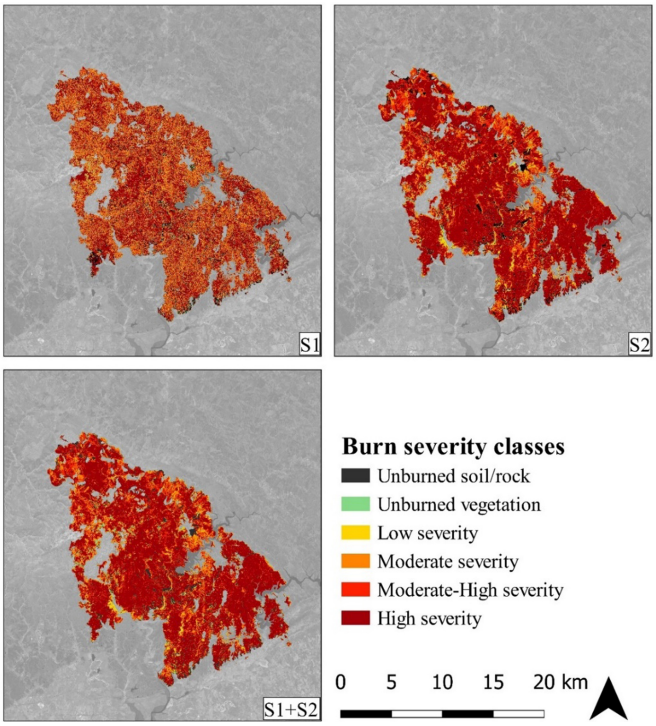

Fig. 2. Burn severity maps resulted from the classification of the three data combination: Sentinel-1 dataset only (S1); Sentinel-2 dataset only (S2); Sentinel-1 and Sentinel-2 data (S1+S2).

4.2 Feature Importance

Each image layer's influence on the classification of each of the three respective data combinations is expressed by the feature importance, whose results are presented below by dividing them by dataset combination. The dataset S1+S2 is reported in Fig. 3; the other two data combinations show almost the same behavior.

Table 5. Distribution (%) of the area of each burn severity class for each data combination: Sentinel-1 dataset only (S1); Sentinel-2 dataset only (S2); S-1 and S-2 data stack (S1+S2).

Burn severity classes	Distribution (%)		
	S1	S2	S1+S2
Unburned soil/rock	6.55	8.35	8.31
Unburned vegetation	11.92	1.85	2.15
Low severity	6.83	2.90	3.03
Moderate severity	17.67	12.54	13.15
Moderate-High severity	16.29	16.84	16.02
High severity	40.74	57.51	57.34

S1. The $BTA_VH_{post\text{-}fire}$ had the highest value of importance (0.1431), followed by its respective ΔBTA_VH image layer (0.1349) and by the VV bands (0.1125 and 0.0983 for ΔBTA_VV and $BTA_VV_{post\text{-}fire}$, respectively). The Δ of the dual-polarimetric indices presented close values of feature importance (from 0.0924 to 0.0886), while the post-fire dual-polarization indices reached a range of values between 0.0814 and 0.0788.

S2. The two-NIR, RedEdge2/3, ΔSWIR2 and Red bands for post-fire ($B8A_{post\text{-}fire}$, $B8_{post\text{-}fire}$, $B7_{post\text{-}fire}$, ΔB12, $B6_{post\text{-}fire}$, $B4_{post\text{-}fire}$) reached the highest values of feature importance: 0.0913, 0.0798, 0.0785, 0.0592, 0.0591 and 0.0554, respectively, followed by the Blue and SWIR2 post-fire (0.0481 and 0.0444). The lowest values are achieved mainly by the NIR-based Δ layers and the RedEdge1 bands (0.0384 to 0.0346).

S1+S2. The feature importance values roughly reflect what has already been seen for individual datasets. The $B8A_{post\text{-}fire}$, $B8_{post\text{-}fire}$, $B7_{post\text{-}fire}$, ΔB12, $B6_{post\text{-}fire}$, $B4_{post\text{-}fire}$ image layers reported highest values: 0.0812, 0.0660, 0.0648, 0.0506, 0.0483, 0.0431, respectively. The $B2_{post\text{-}fire}$ (0.0298) preceded the $B12_{post\text{-}fire}$ (0.0334). The $BTA_VH_{post\text{-}fire}$ reached the fifteenth value of importance (0.0316); the other SAR based, especially both the BTA_VV layers, returned the lowest values.

4.3 Map Accuracy

The accuracy of each map was evaluated using several accuracy metrics, and the resulted values are reported below. The F-score was calculated both for the single classes ($F\text{-}score_i$) to have a more comprehensive measure for each of them and for all the classes ($F\text{-}score_M$), thus expressing the map's overall accuracy. The initial out-of-bag (OOB) error, representing a forecast accuracy performance estimated by the RF model during the training step, was also reported.

S1. Considering the $F\text{-}score_i$ for each class, the values are 0.732 (unburned soil/rock), 0.372 (unburned vegetation), 0.267 (low severity), 0.434 (moderate severity), 0.489 (moderate-high severity), 0.721 (high severity). The overall accuracy expressed by the $F\text{-}score_M$ is 0.513. The OOB error was equal to 0.5101.

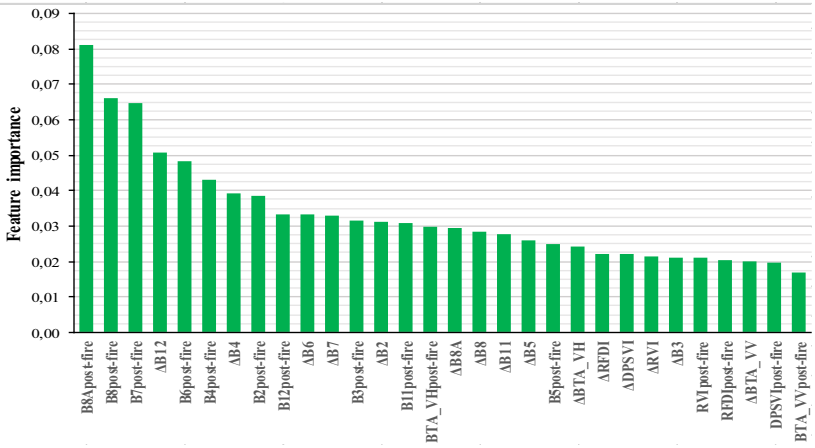

Fig. 3. Feature importance (Gini importance) expressed by each image layer used in the classification process of the Sentinel-1 and Sentinel-2 data stack (S1+S2).

S2. The $F\text{-}score_i$ for each class is 0.933 (unburned soil/rock), 0.879 (unburned vegetation), 0.615 (low severity), 0.683 (moderate severity), 0.773 (moderate-high severity), 0.898 (high severity). The $F\text{-}score_M$ is 0.805. The OOB error was 0.7805.

S1+S2. For each single class, the values of $F\text{-}score_i$ reached are 0.933 (unburned soil/rock), 0.899 (unburned vegetation), 0.696 (low severity), 0.738 (moderate severity), 0.818 (moderate-high severity), 0.916 (high severity). The $F\text{-}score_M$ resulted 0.838. The OOB error was equal to 0.7996.

5 Discussion

This study tested the capability of the integrated use of the two types of SAR (S1) and optical (S2) data in order to map the burn severity in a heterogeneous Mediterranean environment. Few studies have tested and compared the results of the combined use of S1 and S2 for burn mapping and burn severity purposes [48, 50, 51]. The burn severity maps obtained in this study provided a different level of accuracy. Although the optical information could already suffice to map burn severity, thanks to the univocal spectral properties that characterize these effects [25, 26], the use of both types of sensors, with the integration of SAR data, leads to better accuracy values. This confirms what other authors had already observed in their studies, such as Stroppiana et al. [48] for burnt area mapping and Tanase et al. [51] for burn severity mapping, proving the importance of integrated information in burned areas monitoring framework. However, when using only optical data, several factors can be a source of spectral confusion, especially at medium-low severity classes, such as the presence of mixed spectral characteristics within the pixels due, for example, to the mixture of unburned and partially unburned vegetation [33]. Tanase et al. [51] noted that the joint use of optical and SAR data improved the classification of areas unburned or affected with low severity. Other authors also considered the phenological status of vegetation as an element that can lead to errors

(e.g., low photosynthetic activity, summer drought stress, leaves fall) [74–77]. Moreover, ash and smoke encrustations on the green leaves surface can alter the optical spectral reflectance [4].

Considering the performance of only SAR data, we achieved the worst result. In other studies using SAR data, such as Addison et al. [39], a level of 60% of overall accuracy is considered high for this type of data. The better performance of VH polarization, compared to VV polarization, in both data configurations (S1 and S1+S2) confirmed what literature reported [21, 41, 45]. We achieved these results using mono-temporal image layers (pre- or post-fire) in order to understand the contribution of each of those to fire severity estimation. However, the bi-temporal spectral indices were more correlated to CBI field measurements [2, 14]. Moreover, the CBI index could present different correlation performances with different vegetation cover types. Studies demonstrate that the CBI is more correlated with forest areas than with shrubs and herbs [14, 18, 28], indicating that the performance of burn severity assessment may vary as vegetation type varies [32]. The contribution of each input layer was explained using the feature importance analysis. The sensitivity of the NIR and SWIR bands was confirmed [26, 32]. However, it is interesting to observe how the RedEdge, Red and Blue bands were also fundamental in achieving the result. Some authors had already hypothesized this aspect. Filipponi et al. [35] proposed a second version of the burn area index (BAI2), built also using the S2 RedEdge (B6, B7) and the narrower bands. Fernández-Manso et al. [34] tested the suitability of RedEdge-based indices for burn severity estimation, achieving good results. Fernández-García et al. [2] used more spectral information than the other NBR type indices, combining Red, Blue, NIR and SWIR bands, considering them very suitable for initial burn severity assessments across different climatic gradients due to their respective sensitivity to atmospheric aerosols, chlorophyll levels, the cellular structure of the leaves and canopy density, and soil and vegetation moisture.

6 Conclusions

This study aims to assess the potential of integrating SAR data to optical datasets to estimate and map burn severity and contribute to the state of the art. The integration improved the accuracy of the results. A more in-depth investigation would be helpful to understand how these data can effectively complete the derived information. In the present work, the various types of vegetation cover were not distinguished. For example, a high severity was attributed without distinction to both pastures, shrubs and forests, as required by the CBI protocol. Future studies could investigate the correlations between severity mapped and vegetation type, an essential key in post-fire monitoring and management of forest regeneration processes and spatial patterns.

Acknowledgments. Giandomenico De Luca was supported by the European Commission through the European Social Fund (ESF) and the Regione Calabria. The authors thank Francisca C. Aguiar (School of Agriculture, University of Lisbon) and Neil E. Pettit (University of Western Australia) for their participation in the fieldwork done in Monchique in the framework of the project RIPONFIRE: Riparian forests: firebreaks or wicks to fire spread?, where the photographs used in this work were taken. RIPONFIRE was funded by the Forest Research Centre,

School of Agriculture, University of Lisbon. The Forest Research Centre is a research unit funded by Fundação para a Ciência e a Tecnologia I.P. (FCT), Portugal (UIDB/00239/2020).

References

1. Chuvieco, E.: Earth Observation of Wildland Fires in Mediterranean Ecosystems. Springer, Berlin Heidelberg (2009), https://doi.org/10.1007/978-3-642-01754-4
2. Fernández-García, V., Santamarta, M., Fernández-Manso, A., Quintano, C., Marcos, E., Calvo, L.: Burn severity metrics in fire-prone pine ecosystems along a climatic gradient using Landsat imagery. Remote Sens. Environ. **206**, 205–217 (2018). https://doi.org/10.1016/j.rse.2017.12.029
3. Lanorte, A., Danese, M., Lasaponara, R., Murgante, B.: Multiscale mapping of burn area and severity using multisensor satellite data and spatial autocorrelation analysis. Int. J. Appl. Earth Obs. Geoinf. **20**, 42–51 (2013). https://doi.org/10.1016/j.jag.2011.09.005
4. Saulino, L., et al.: Detecting burn severity across Mediterranean forest types by coupling medium-spatial resolution satellite imagery and field data. Remote Sens. **12**, 1–21 (2020), https://doi.org/10.3390/rs12040741
5. San-Miguel-Ayanza, J., et al.: Forest fires in Europe, Middle East and North Africa 2018. JRC Technical Report. Publications Office of the European Union (2019), https://doi.org/10.2760/1128
6. Silva, J.M.N., Moreno, M.V., Le Page, Y., Oom, D., Bistinas, I., Pereira, J.M.C.: Spatiotemporal trends of area burnt in the Iberian Peninsula, 1975–2013. Reg. Environ. Change **19**(2), 515–527 (2018). https://doi.org/10.1007/s10113-018-1415-6
7. Mitri, G.H., Gitas, I.Z.: Mapping post-fire forest regeneration and vegetation recovery using a combination of very high spatial resolution and hyperspectral satellite imagery. Int. J. Appl. Earth Obs. Geoinf. **20**, 60–66 (2012). https://doi.org/10.1016/j.jag.2011.09.001
8. Häusler, M., et al.: Assessment of the indirect impact of wildfire (severity) on actual evapotranspiration in eucalyptus forest based on the surface energy balance estimated from remote-sensing techniques. Int. J. Remote Sens. **39**, 6499–6524 (2018). https://doi.org/10.1080/01431161.2018.1460508
9. Modica, G., Merlino, A., Solano, F., Mercurio, R.: An index for the assessment of degraded Mediterranean forest ecosystems. For. Syst. (2015). https://doi.org/10.5424/fs/2015243-07855
10. Morresi, D., Vitali, A., Urbinati, C., Garbarino, M.: Forest spectral recovery and regeneration dynamics in stand-replacing wildfires of central Apennines derived from Landsat time series. Remote Sens. 11 (2019), https://doi.org/10.3390/rs11030308
11. Semeraro, T., Vacchiano, G., Aretano, R., Ascoli, D.: Application of vegetation index time series to value fire effect on primary production in a Southern European rare wetland. Ecol. Eng. **134**, 9–17 (2019). https://doi.org/10.1016/j.ecoleng.2019.04.004
12. Di Fazio, S., Modica, G., Zoccali, P.: Evolution trends of land use/land cover in a mediterranean forest landscape in Italy. In: Murgante, B., et al. (eds.) Computational Science and Its Applications - ICCSA 2011. ICCSA 2011. LNCS, vol. 6782, pp. 284–299. Springer, Berlin, Heidelberg (2011). https://doi.org/10.1007/978-3-642-21928-3_20
13. Keeley, J.E.: Fire intensity, fire severity and burn severity: a brief review and suggested usage. Int. J. Wildl. Fire. **18**, 116–126 (2009). https://doi.org/10.1071/WF07049
14. Key, C.H., Benson, N.C.: Landscape Assessment (LA) sampling and analysis methods. In: FIREMON: Fire Effects Monitoring and Inventory System (2006)

15. De Luca, G., Modica, G., Fattore, C., Lasaponara, R.: Unsupervised Burned Area Mapping in a Protected Natural Site. An Approach Using SAR Sentinel-1 Data and K-mean Algorithm. In: Gervasi, O., et al. (eds.) ICCSA 2020. LNCS, vol. 12253, pp. 63–77. Springer, Cham (2020). https://doi.org/10.1007/978-3-030-58814-4_5
16. Gitas, I., Mitri, G., Veraverbeke, S., Polychronaki, A.: Advances in remote sensing of post-fire vegetation recovery monitoring - a review. Remote Sens. Biomass - Princ. Appl. (2012). https://doi.org/10.5772/20571
17. Meng, R., Wu, J., Zhao, F., Cook, B.D., Hanavan, R.P., Serbin, S.P.: Measuring short-term post-fire forest recovery across a burn severity gradient in a mixed pine-oak forest using multi-sensor remote sensing techniques. Remote Sens. Environ. **210**, 282–296 (2018). https://doi.org/10.1016/j.rse.2018.03.019
18. De Santis, A., Chuvieco, E.: GeoCBI: A modified version of the Composite Burn Index for the initial assessment of the short-term burn severity from remotely sensed data. Remote Sens. Environ. **113**, 554–562 (2009). https://doi.org/10.1016/j.rse.2008.10.011
19. Otón, G., Ramo, R., Lizundia-Loiola, J., Chuvieco, E.: Global detection of long-term (1982–2017) burned area with AVHRR-LTDR data. Remote Sens. **11** (2019), https://doi.org/10.3390/rs11182079
20. De Santis, A., Chuvieco, E.: Burn severity estimation from remotely sensed data: performance of simulation versus empirical models. Remote Sens. Environ. **108**, 422–435 (2007). https://doi.org/10.1016/j.rse.2006.11.022
21. Tanase, M.A., Kennedy, R., Aponte, C.: Radar Burn Ratio for fire severity estimation at canopy level: an example for temperate forests. Remote Sens. Environ. **170**, 14–31 (2015). https://doi.org/10.1016/j.rse.2015.08.025
22. Chuvieco, E., et al.: Historical background and current developments for mapping burned area from satellite Earth observation. Remote Sens. Environ. **225**, 45–64 (2019). https://doi.org/10.1016/j.rse.2019.02.013
23. Praticò, S., Solano, F., Di Fazio, S., Modica, G.: Machine learning classification of Mediterranean forest habitats in google earth engine based on seasonal sentinel-2 time-series and input image composition optimisation. Remote Sens. **13**, 1–28 (2021)
24. ESA Sentinel Homepage (2021): https://sentinels.copernicus.eu/web/sentinel/home. Accessed 11 Mar 2021
25. Silva, J.M.N., Cadima, J.F.C.L., Pereira, J.M.C., Grégoire, J.M.: Assessing the feasibility of a global model for multi-temporal burned area mapping using SPOT-VEGETATION data. Int. J. Remote Sens. (2004)
26. Pereira, J.M.C., Sá, A.C.L., Sousa, A.M.O., Silva, J.M.N., Santos, T.N., Carreiras, J.M.B.: Spectral characterisation and discrimination of burnt areas. Remote Sens. Large Wildfires (1999). https://doi.org/10.1007/978-3-642-60164-4_7
27. Cansler, C.A., McKenzie, D.: How robust are burn severity indices when applied in a new region? Evaluation of alternate field-based and remote-sensing methods. Remote Sens. **4**, 456–483 (2012). https://doi.org/10.3390/rs4020456
28. Epting, J., Verbyla, D., Sorbel, B.: Evaluation of remotely sensed indices for assessing burn severity in interior Alaska using Landsat TM and ETM+. Remote Sens. Environ. (2005). https://doi.org/10.1016/j.rse.2005.03.002
29. Fornacca, D., Ren, G., Xiao, W.: Evaluating the best spectral indices for the detection of burn scars at several post-fire dates in a Mountainous Region of Northwest Yunnan, China. Remote Sens. **10** (2018), https://doi.org/10.3390/rs10081196
30. Mallinis, G., Mitsopoulos, I., Chrysafi, I.: Evaluating and comparing sentinel 2A and landsat-8 operational land imager (OLI) spectral indices for estimating fire severity in a Mediterranean pine ecosystem of Greece. GIScience Remote Sens. (2018)

31. De Santis, A., Chuvieco, E., Vaughan, P.J.: Short-term assessment of burn severity using the inversion of PROSPECT and GeoSail models. Remote Sens. Environ. **113**, 126–136 (2009). https://doi.org/10.1016/j.rse.2008.08.008
32. Schepers, L., et al..: Burned area detection and burn severity assessment of a heathland fire in Belgium using airborne imaging spectroscopy (APEX). Remote Sens. **6**, 1803–1826 (2014)
33. Quintano, C., Fernández-Manso, A., Roberts, D.A.: Multiple endmember spectral mixture analysis (MESMA) to map burn severity levels from Landsat images in Mediterranean countries. Remote Sens. Environ. **136**, 76–88 (2013)
34. Fernández-Manso, A., Fernández-Manso, O., Quintano, C.: SENTINEL-2A red-edge spectral indices suitability for discriminating burn severity. Int. J. Appl. Earth Obs. Geoinf. (2016). https://doi.org/10.1016/j.jag.2016.03.005
35. Filipponi, F.: BAIS2: Burned Area Index for Sentinel-2. 5177 (2018)
36. Miller, J.D., et al.: Calibration and validation of the relative differenced Normalized Burn Ratio (RdNBR) to three measures of fire severity in the Sierra Nevada and Klamath Mountains, California, USA. Remote Sens. Environ. **113**, 645–656 (2009)
37. Parks, S.A., Dillon, G.K., Miller, C.: A new metric for quantifying burn severity: the relativized burn ratio. Remote Sens. **6**, 1827–1844 (2014). https://doi.org/10.3390/rs6031827
38. Zheng, Z., Zeng, Y., Li, S., Huang, W.: A new burn severity index based on land surface temperature and enhanced vegetation index. Int. J. Appl. Earth Obs. Geoinf. (2016). https://doi.org/10.1016/j.jag.2015.11.002
39. Addison, P., Oommen, T.: Utilizing satellite radar remote sensing for burn severity estimation. Int. J. Appl. Earth Obs. Geoinf. (2018)
40. Kurum, M.: C-Band SAR Backscatter Evaluation of 2008 Gallipoli Forest Fire. **12**, 1091–1095 (2015)
41. Lasaponara, R., Tucci, B.: Identification of burned areas and severity. IEEE Geosci. Remote Sens. Lett. **16**, 917–921 (2019). https://doi.org/10.1109/LGRS.2018.2888641
42. Tanase, M.A., Santoro, M., Aponte, C., De La Riva, J.: Polarimetric properties of burned forest areas at C- and L-band. IEEE J. Sel. Top. Appl. Earth Obs. Remote Sens. (2014), https://doi.org/10.1109/JSTARS.2013.2261053
43. Tanase, M.A., Santoro, M., Wegmüller, U., de la Riva, J., Pérez-Cabello, F.: Properties of X-, C- and L-band repeat-pass interferometric SAR coherence in Mediterranean pine forests affected by fires. Remote Sens. Environ. (2010a)
44. Tanase, M.A., Santoro, M., De La Riva, J., Pérez-Cabello, F., Le Toan, T.: Sensitivity of X-, C-, and L-band SAR backscatter to burn severity in Mediterranean pine forests. IEEE Trans. Geosci. Remote Sens. **48**, 3663–3675 (2010)
45. Imperatore, P., Azar, R., Calo, F., Stroppiana, D., Brivio, P.A., Lanari, R., Pepe, A.: Effect of the vegetation fire on backscattering: an investigation based on Sentinel-1 observations. IEEE J. Sel. Top. Appl. Earth Obs. Remote Sens. **10**, 4478–4492 (2017), https://doi.org/10.1109/JSTARS.2017.2717039
46. Lasko, K.: Incorporating Sentinel-1 SAR imagery with the MODIS MCD64A1 burned area product to improve burn date estimates and reduce burn date uncertainty in wildland fire mapping. Geocarto Int. 1–21 (2019), https://doi.org/10.1080/10106049.2019.1608592
47. Lehmann, E.A., et al.: SAR and optical remote sensing: assessment of complementarity and interoperability in the context of a large-scale operational forest monitoring system. Remote Sens. Environ. **156**, 335–348 (2015)
48. Stroppiana, D., et al.: Integration of optical and SAR data for burned area mapping in Mediterranean regions. Remote Sens. **7**, 1320–1345 (2015)
49. De Luca, G., Silva, J.M.N., Modica, G.: A workflow based on Sentinel-1 SAR data and open-source algorithms for unsupervised burned area detection in Mediterranean ecosystems. GIScience Remote Sens. **00**, 1–26 (2021)

50. Verhegghen, A., et al.: The potential of sentinel satellites for burnt area mapping and monitoring in the Congo Basin forests. Remote Sens. **8**, 1–22 (2016)
51. Tanase, M.A., Kennedy, R., Aponte, C.: Fire severity estimation from space: a comparison of active and passive sensors and their synergy for different forest types. Int. J. Wildl. Fire. **24**, 1062–1075 (2015). https://doi.org/10.1071/WF15059
52. The Python Language Reference (2021): https://docs.python.org/3/reference/. Accessed 15 Mar 2021
53. Sistema Nacional de Informação Geográfica (SNIG) (2021): https://snig.dgterritorio.gov.pt/. Accessed 15 Mar 2021
54. Copernicus Open Access Hub (2021): https://scihub.copernicus.eu/. Accessed 15 Mar 2021
55. Esri ArcGIS World Imagery (2021): https://www.arcgis.com/home/item.html?id=10df2279f9684e4a9f6a7f08febac2a9. Accessed 19 Mar 2021
56. ESA SNAP Homepage (2021): http://step.esa.int/main/toolboxes/snap/. Accessed 11 Mar 2021
57. ESA SNAP Cookbook (2021): https://senbox.atlassian.net/wiki/spaces/SNAP/pages/24051769/Cookbook
58. Quegan, S., Toan, T.L., Yu, J.J., Ribbes, F., Floury, N.: Multitemporal ERS SAR analysis applied to forest mapping. IEEE Trans. Geosci. Remote Sens. (2000). https://doi.org/10.1109/36.842003
59. Santoso, A.W., Pebrianti, D., Bayuaji, L., Zain, J.M.: Performance of various speckle reduction filters on Synthetic Aperture Radar image. In: 2015 4th Int. Conf. Softw. Eng. Comput. Syst. ICSECS 2015 Virtuous Softw. Solut. Big Data, pp. 11–14 (2015)
60. Mandal, D., et al.: Remote sensing of environment dual polarimetric radar vegetation index for crop growth monitoring using sentinel-1 SAR data. Remote Sens. Environ. **247**, 111954 (2020). https://doi.org/10.1016/j.rse.2020.111954
61. Nasirzadehdizaji, R., Sanli, F.B., Abdikan, S., Cakir, Z., Sekertekin, A., Ustuner, M.: Sensitivity analysis of multi-temporal Sentinel-1 SAR parameters to crop height and canopy coverage. Appl. Sci. (2019). https://doi.org/10.3390/app9040655
62. Nicolau, A.P., Flores-Anderson, A., Griffin, R., Herndon, K., Meyer, F.J.: Assessing SAR C-band data to effectively distinguish modified land uses in a heavily disturbed Amazon forest. Int. J. Appl. Earth Obs. Geoinf. **94**, 102214 (2021). https://doi.org/10.1016/j.jag.2020.102214
63. Breiman, L.: Random forests. Mach. Learn. **45**, 5–32 (2001)
64. Cutler, D.R., et al.: Random forests for classification in ecology. Ecology **88**, 2783–2792 (2007)
65. Pedregosa, F., et al.: Scikit-learn: machine learning in Python. J. Mach. Learn. Res. **12**, 2825–2830 (2011)
66. Congalton, R.G., Green, K.: Assessing the Accuracy of Remotely Sensed Data. Principles and Practices (2019)
67. Goutte, C., Gaussier, E.: A Probabilistic Interpretation of Precision, Recall and F-Score, with Implication for Evaluation. In: Losada, D.E., Fernández-Luna, J.M. (eds.) ECIR 2005. LNCS, vol. 3408, pp. 345–359. Springer, Heidelberg (2005). https://doi.org/10.1007/978-3-540-31865-1_25
68. Ok, A.O., Senaras, C., Yuksel, B.: Automated detection of arbitrarily shaped buildings in complex environments from monocular VHR optical satellite imagery. IEEE Trans. Geosci. Remote Sens. **51**, 1701–1717 (2013)
69. Shufelt, J.A.: Performance evaluation and analysis of monocular building extraction from aerial imagery. IEEE Trans. Pattern Anal. Mach. Intell. **21**, 311–326 (1999)
70. Sokolova, M., Japkowicz, N., Szpakowicz, S.: Beyond Accuracy, F-Score and ROC: A Family of Discriminant Measures for Performance Evaluation. In: Sattar, A., Kang, B.-h (eds.) AI 2006. LNCS (LNAI), vol. 4304, pp. 1015–1021. Springer, Heidelberg (2006). https://doi.org/10.1007/11941439_114

71. Modica, G., Messina, G., De Luca, G., Fiozzo, V., Praticò, S.: Monitoring the vegetation vigor in heterogeneous citrus and olive orchards. A multiscale object-based approach to extract trees' crowns from UAV multispectral imagery. Comput. Electron. Agric. **175**, 105500 (2020)
72. Sokolova, M., Lapalme, G.: A systematic analysis of performance measures for classification tasks. Inf. Process. Manag. **45**, 427–437 (2009)
73. Modica, G., De Luca, G., Messina, G., Praticò, S.: Comparison and assessment of different object-based classifications using machine learning algorithms and UAVs multispectral imagery in the framework of precision agriculture. Eur. J. Remote Sens. **54**, 431–460 (2021). https://doi.org/10.1080/22797254.2021.1951623
74. Gallagher, M.R., et al.: An improved approach for selecting and validating burn severity indices in forested landscapes an improved approach for selecting and validating burn severity indices in feux dans des milieux forestiers. Can. J. Remote Sens. **46**, 100–111 (2020). https://doi.org/10.1080/07038992.2020.1735931
75. Inoue, Y., et al.: Reflectance characteristics of major land surfaces in slash - and - burn ecosystems in Laos. 1161 (2019), https://doi.org/10.1080/01431160701442039
76. Picotte, J.J., Robertson, K.M.: Validation of remote sensing of burn severity in south-eastern US ecosystems. Int. J. Wildl. Fire. (2011). https://doi.org/10.1071/WF10013
77. Verbyla, D.L.V., Kasischke, E.S.K., Hoy, E.E.H.: Seasonal and topographic effects on estimating fire severity from Landsat TM/ETM + data. 527–534 (2008)